Railway Sciences

647

Received 3 July 2025
Revised 11 August 2025
Accepted 4 September 2025

A clip-on composite sensor based packaging design method for fiber Bragg grating axle counter

Mengyao Zhao
China Academy of Railway Sciences Corporation Limited, Communication and Signaling Research Institute, Beijing, China
Xueyun Cao
Department of Optoelectronic Science and Engineering, China University of Petroleum East China, Qingdao, China
Longsheng Wang and Yang Peng
China Academy of Railway Sciences Corporation Limited, Communication and Signaling Research Institute, Beijing, China, and
Tao Wang
Department of Optoelectronic Science and Engineering, China University of Petroleum East China, Qingdao, China

Abstract

Purpose – To address the encapsulation challenge of fiber Bragg grating (FBG) sensors in complex railway environments, this paper designs a clip-on composite sensor enabling installation-friendly deployment and long-term axle counting system monitoring.

Design/methodology/approach – Wheel–rail mechanical behavior was simulated via finite element analysis (FEA) to determine optimal sensor placement. A clip-on composite sensor was subsequently engineered. Stress transduction efficacy was validated through FEA quantification of stress responses at the axle counter location.

Findings – The proposed FBG axle counter integrates temperature compensation and anti-detachment monitoring as well as advantages such as simplified installation with minimal maintenance and sustained operational reliability. It effectively transmits stress, yielding a measured strain of 39 με under static loading conditions without sensitivity-enhancing elements.

Originality/value – This study performs FEA of wheel-rail stress distribution and engineers the dual-slot composite sensor, FEA was conducted to quantify the stress magnitude at the axle sensor position of the dual-slot composite sensor. Additionally, FEA was performed on sensors with different structural configurations, including adjustments to the axle sensor position, number of slots and axle position. The results confirmed that the designed composite sensor exhibits superior stress transfer characteristics.

Keywords Fiber Bragg grating, Axle counting, Finite element, Sensor, Wheel–rail forces

Paper type Research article

1. Introduction

Axle counting technology utilizes sensors to detect axle information from passing trains, calculating axle numbers for track occupancy monitoring by comparing counts at both ends of a monitored section. Current systems predominantly employ electromagnetic axle counters that detect wheel passages via track-mounted sensors. While this equipment offers operational simplicity and broad adoption (Liu, 2019), its components exhibit inadequate moisture

Railway Sciences
Vol. 4 No. 5, 2025
pp. 647-665
Emerald Publishing Limited
e-ISSN: 2755-0915
p-ISSN: 2755-0907
DOI 10.1108/RS-07-2025-0023

resistance, corrosion resistance, and electromagnetic interference (EMI) resilience under harsh conditions (Ding, Zhao, Cheng, & Du, 2024). Moreover, each electromagnetic head requires pre-embedded power cables, rendering deployment in unmanned sections impractical.

Fiber Bragg gratings (FBGs) possess inherent advantages including compact size, strong EMI immunity, and low long-distance transmission loss (Canning, 2008). FBG sensing networks deployed along tracks operate without external power supplies, transmitting only optical signals. This enables stable performance in complex railway environments and facilitates axle counting applications (Kacik, Martincek, Maciak, & Goraus, 2022). Therefore, many researchers have conducted extensive theoretical and experimental explorations on this topic. Lee, Lee, and Ho (2004) designed an FBG axle counter identifying trains through axle spacing, weight, and carriage number variations. Liu, Jian, Pei, and Yan (2005) installed multi-wavelength FBG sensors to locate trains via wavelength shift detection, validating efficacy through engineering implementations. Li, Pan, and Fan (2009) proposed a wavelength-based fiber optic grating axis sensing system that uses wavelength division multiplexing technology to achieve distributed sensing of multiple grating sensors. Wei *et al.* (2010) developed a differential-principle FBG sensor measuring rail strain. Yan *et al.* (2011) demonstrated external strain measurement reliability via FBG mounting optimization and reflected power detection. Yu, He, Wang, and Wang (2014) enhanced sensor robustness through tri-sensor collocation and peak-detection algorithms, accommodating variable train speeds. Zhang and Yan (2019) implemented Gaussian-polynomial fitting and cumulative-influence algorithms for axle counting and direction identification. Zhang *et al.* (2020) achieved high-speed demodulation using optical couplers and filters. Pan *et al.* (2022) employed dual high-sensitivity FBG strain sensors for axle counting and direction determination. Wu *et al.* (2024) partitioned the system into sensing, demodulation, and control subsystems for universal applicability across operational scenarios.

Finite element analysis (FEA) constitutes an engineering simulation methodology grounded in numerical approximation techniques. Leveraging mathematical principles and computational algorithms, it provides a robust framework for solving complex engineering problems. The core paradigm involves mathematical discretization of physical systems–encompassing geometry, material properties, and boundary conditions–into finite interconnected elements. This approach approximates continuum systems with infinite degrees of freedom through finite-dimensional subspace representations governed by variational principles. Hajar and Mounia (2025) analyzed the sensitivity of parameters such as contact pressure, contact patch, shear stress, stick-slip transition zones, and von Mises stress under different operating conditions for ballasted and ballastless. Wang, Zhou, Liu, Wang, and Jing (2025) investigated the time-domain and frequency-domain responses of wheel-rail contact force, wheel-rail adhesion/slip distribution, and stress states during wheel rolling in tread defect regions, and predicted wheel-rail plastic deformation and wear damage. He, Wang, Zhang, Wang, and Yang (2024) simulated the stress and strain distributions at wheel-rail contact points when C80 freight cars passed through various corrugated sections of heavy-haul railways with varying wavelengths and wave depths. Cai, Chen, and Chang (2024) employed FEA to characterize stress-strain distributions across the railhead under varying wheel-rail force regimes, identifying optimal strain gauge placement for wheel-rail force monitoring systems. Velic *et al.* (2023) developed a dynamic 3D finite element model, quantifying transient stress and plastic strain evolution in switch rails.

Despite these advances, existing research primarily focuses on modeling and algorithm optimization, with insufficient attention to field-application-oriented sensor structural design. The complexity of railway environments imposes significant challenges on FBG encapsulation. Environmental factors–including thermal fluctuations, humidity variations, mechanical vibrations, and strong EMI–can degrade measurement accuracy and long-term stability. Thus, rational encapsulation design is critical for enhancing FBG reliability,

durability, and precision in railway monitoring, forming the foundation for sustained operational integrity. Numerous investigators have employed FEA to examine wheel-rail interactions, including contact mechanics and force transmission dynamics. These studies substantiate the efficacy of FEA in modeling railway wheel-rail interface behaviors.

This study addresses the inadequacy of current FBG axle counter encapsulation in complex railway environments. The axle counting principle is briefly introduced, followed by FEA of wheel-rail stress interactions to determine optimal sensor placement. Based on these findings, this study designs a composite sensor featuring installation-friendly architecture and long-term monitoring capability. Further FEA quantifies stress distribution in the axle counter, validating effective stress transfer within the composite structure.

2. FEA of FBG sensor wheel-rail interaction

The sensing principle of FBGs relies on their wavelength-specific reflectance characteristics: incident light undergoes selective reflection at a particular Bragg wavelength. Variations in ambient physical quantities–such as temperature, strain, or stress–alter the grating period and/or the effective core refractive index. This wavelength shift is governed by the fundamental equation, as follows (Ni, 2022):

$$\lambda_B = 2n_{eff}\Lambda \tag{1}$$

In the equation, λ_B is the FBG wavelength; n_{eff} is the core refractive index, typically a constant; Λ is the grating period. Leveraging the strain-sensing capability of FBGs, rail deformation induced by train wheel-sets can be quantitatively monitored. During train passage, FBGs detect dynamic strain pulses characterized by distinct peak profiles. This pulse signature establishes the fundamental mechanism for FBG-based axle counting. To characterize the strain response profile of FBGs during axle passage, precise quantification of rail strain transients and spatial strain distribution under wheel loading is essential. Employing FEA to examine rail stress-strain behavior and deformation during train transit constitutes an effective methodology. Consequently, finite element software was utilized to develop high-fidelity wheel-rail models for further investigation of train-track interaction mechanisms. During modeling, constitutive material properties, geometric configurations, and boundary conditions were rigorously incorporated to ensure accurate representation of in-service wheel-rail performance. Analysis of region-specific stress-strain distributions enables precise identification of critical zones exhibiting stress concentrations and significant strain transients. FBG sensors deployed in these zones establish the foundation for axle counting functionality. Furthermore, FEA-derived data inform sensor design optimization.

3. FEA of wheel-rail interaction

The fundamental workflow of FEA comprises three sequential phases: preprocessing, solution, and postprocessing. Initially, the computational domain is established through geometric modeling and discretization of the analysis object. Subsequently, boundary conditions and applied loads are defined in accordance with physical constraints. Ultimately, the obtained solution is analyzed and evaluated. Based on operational parameters of China's passenger rail services, a finite element model was established incorporating a standard 60 kg/m rail profile and CRH2 EMU wheel set as shown in Figure 1. The wheel tread is of the LMA type, and the rail is set with a 1:40 rail base slope. This study adopts a unified coordinate system orientation with the x-axis aligned transversely to the rail, the y-axis parallel to the longitudinal direction, and the z-axis normal to the vertical plane. Boundary conditions are set for the wheel-rail system: the wheel axle position is fixed in the x and y directions, a vertical downward load of 100 kN is applied to the wheel, the friction coefficient at the wheel-rail contact surface is set to 0.2, and the track bottom boundary segments at both ends are fixed.

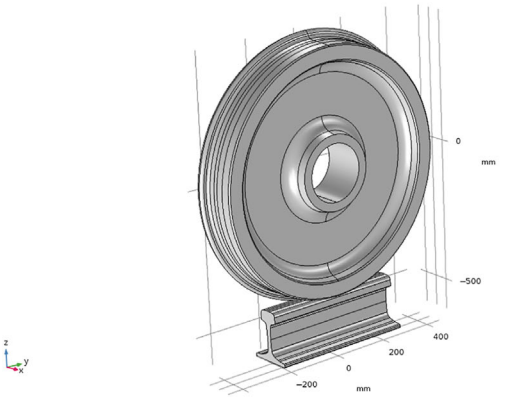

Figure 1. Wheel–rail model. **Source(s):** Authors' own work

The rail length is set to the sleeper spacing, simplifying the track into a simply supported beam model. The material properties of the wheel and rail are shown in Table 1. Discretization of the continuous wheel-rail model involves mesh generation. Given the complex contact mechanics at the wheel-rail interface, the contact zone mesh is refined, while mesh density decreases inversely proportional to distance from the contact region. The rail and wheel mesh configurations are illustrated in Figures 2 and 3 respectively. Figure 4 shows the equivalent stress of the wheel and rail obtained through finite element simulation, with a maximum equivalent stress of 1,240 N/m^2. Under mid-span vertical loading, the stress field exhibits bilateral symmetry about the vertical plane through the load point, with compressive stresses developing in the upper region of the rail and tensile stresses arising in the lower region. The locations with higher equivalent stress on the rail include the rail head, rail web, and rail base. FEA reveals a distinct stress gradient across rail sections: the rail head exhibits the highest equivalent stress, followed by the web, with the base showing the lowest magnitude. However, considering long-term sensor deployment requirements, the rail head experiences significant stress fluctuations under dynamic loads, while sensor installation in this zone risks interfering with train operations. Additionally, the rail web is unsuitable due to constrained installation space and method limitations.

To determine the optimal FBG alignment, stress tensor components along x-(lateral), y-(longitudinal), and z-(vertical) axes in the rail are presented in Figures 5–7. Stress test points with significant deformation were selected for each section of the rail. For the rail head, a point on the inferior surface of the rail head was selected; for the rail web, a point along the central axis with higher stress was selected; and for the rail bottom, a point at the center of the bottom was selected. Equivalent von Mises stress and directional stress tensor components (x, y, z)

Table 1. Wheel-rail material properties

Model	Density (kg/m3)	Young's modulus (N/m^2)	Poisson's ratio
Rails	7,850	200,000	0.3
Wheels	7,850	200,000	0.3

Source(s): Authors' own work

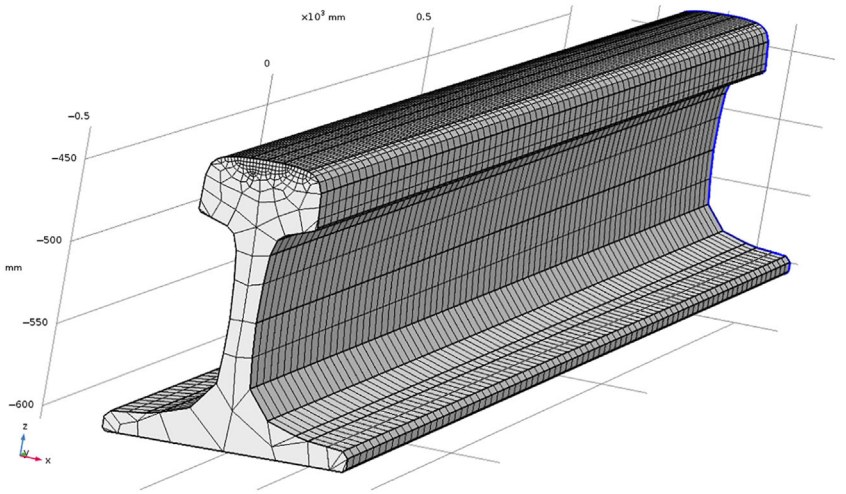

Figure 2. Rail mesh configurations. **Source(s):** Authors' own work

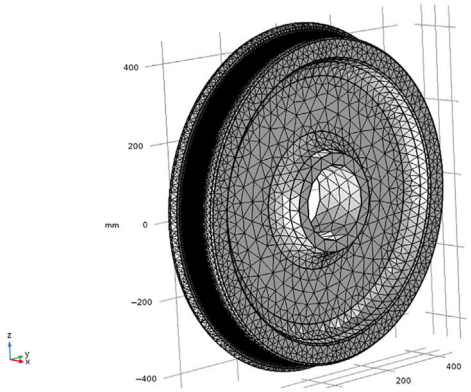

Figure 3. Wheel mesh configurations. **Source(s):** Authors' own work

were quantified at these measurement points as documented in Table 2. Analyze the stress field in areas outside the load application location. The transverse stress peaks beneath the load and at sleeper supports; the longitudinal stress dominates at mid-span with compression beneath the load and tension adjacent to it; the vertical stress component exhibits significant magnitude in the rail web, with compressive stress developing beneath the applied load and tensile stress manifesting on both transverse sides of the load zone. Comparative analysis of stress magnitudes at the rail base reveals the dominant order: $\sigma_y > \sigma_z > \sigma_x$ (where σ denotes stress), and the tensile strain in the y direction was significantly greater than that in the x and z directions. Consequently, aligning the FBG sensor axis parallel to the longitudinal y-direction constitutes the optimal deployment configuration for strain transduction efficiency.

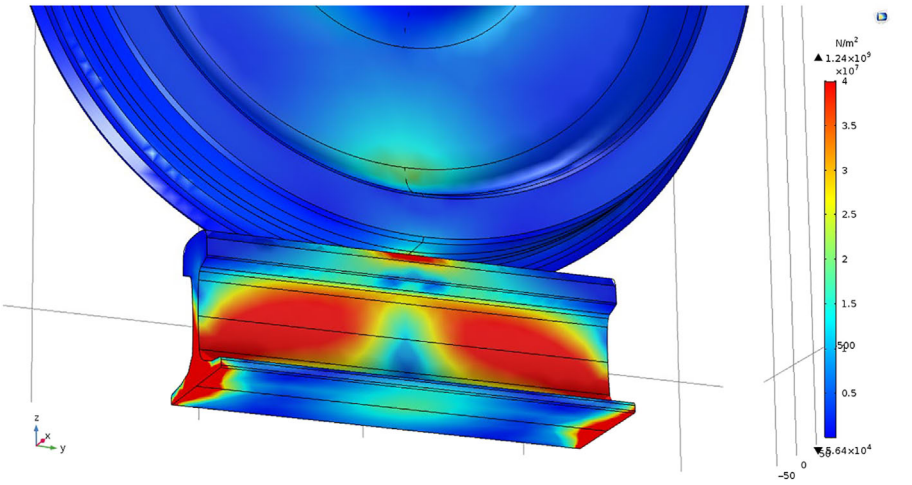

Figure 4. Equivalent stress on wheels and rails. **Source(s):** Authors' own work

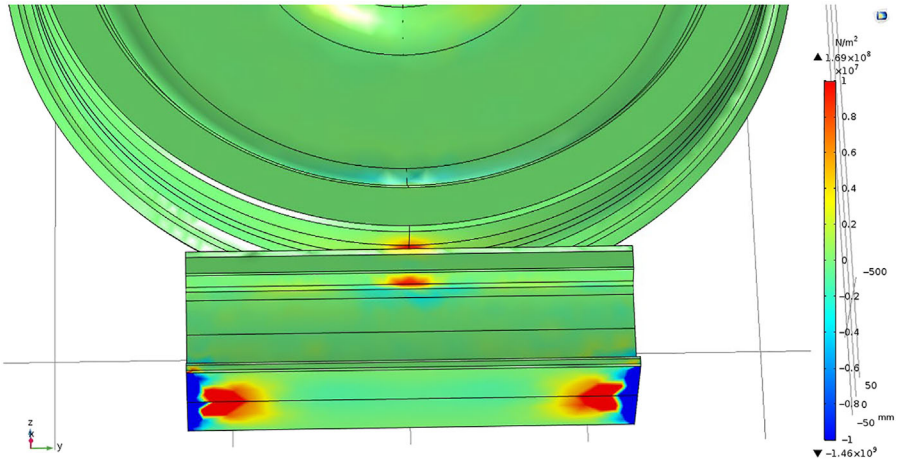

Figure 5. x component of orbital stress tensor. **Source(s):** Authors' own work

4. Sensor design

Current FBG encapsulation methods comprise adhesive bonding, welding, and clip-on clamping. While organic adhesives suffice for general applications, their susceptibility to creep and aging compromises long-term stability under complex environmental conditions. Specifically in railway environments–characterized by significant thermal cycling, high humidity, and persistent mechanical vibrations–adhesive-based FBG encapsulation fails to ensure sustained operational reliability. For axle counting applications, although welding provides robust fixation, its inherent destructive installation risks track integrity damage and incurs high maintenance costs, limiting practical deployment. In contrast, clip-on sensors deliver flexible installation without structural compromise while maintaining measurement stability.

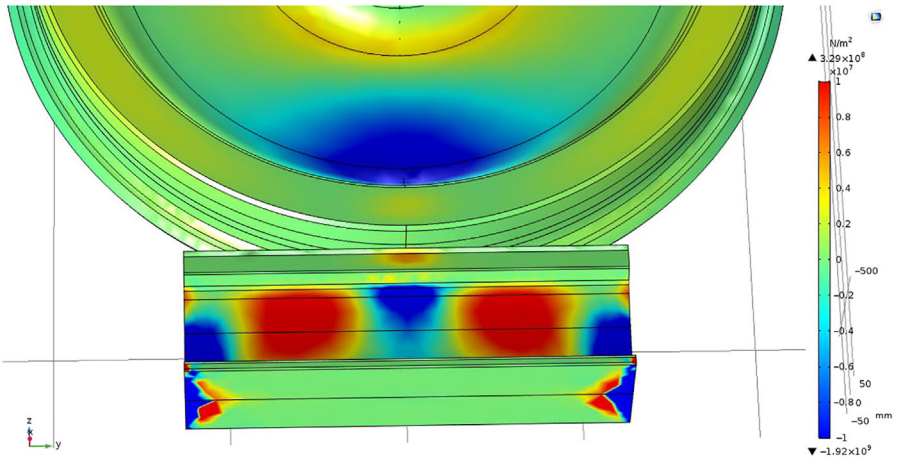

Figure 6. y component of orbital stress tensor. **Source(s):** Authors' own work

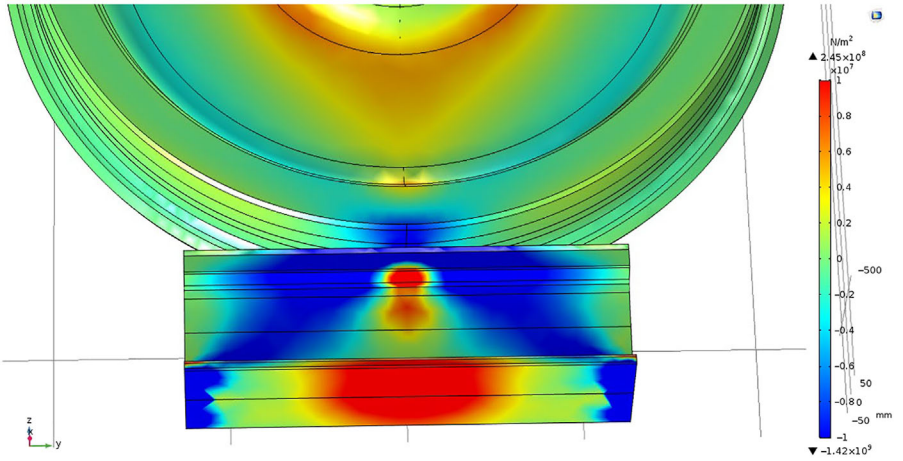

Figure 7. z component of orbital stress tensor. **Source(s):** Authors' own work

Table 2. Stress distribution of rails

Stress	Rail head (N/m^2)	Rail web (N/m^2)	Rail base (N/m^2)
Von mises	30.3	46.9	17.2
X-	10.3	−0.5	−0.7
Y-	34.0	−16.7	17.5
Z-	−47.2	−52.7	−0.2

Source(s): Authors' own work

Based on the stress transfer relationship between the wheel and rail described earlier, a clip-on sensor was engineered, as shown in the Figure 8. The composite sensor is equipped with five fiber optic grating sensors. Two anti-loosening monitoring FBGs perpendicular to the rail *y*-axis (lateral grooves), detecting installation integrity and triggering maintenance alerts. Two axle-counting FBGs parallel to *y*-axis and one temperature-compensating FBG perpendicular to the *y*-axis (central zone), eliminating thermal interference. The FBG is bonded to the strain gauge using polymer adhesive, and the strain gauge is permanently affixed to the steel plate through welding. Clamps on both sides apply compressive force to the central steel plate, secured with bolts. The FBG is positioned within the groove between the plate and rail base, as shown in Figure 9. To enhance strain transfer efficiency, a thickness reduction was implemented at the grating location, thus increasing strain sensitivity, as shown in Figure 10.

Experimental testing revealed suboptimal sensor performance. Analysis indicated that this was likely attributable to bolt fastening predominantly constraining movement in the *x*-direction, providing insufficient constraint in the *z*-direction, coupled with significant stress transmission loss within the steel plate structure. To address these issues, structural optimizations were implemented:

(1) Slots were introduced into the steel plate to enhance sensitivity, as depicted in the Figure 11;

(2) A base was incorporated between the axle counting sensor and the steel plate, also serving to enhance sensitivity (as depicted in the Figure 12);

(3) Eight additional screws and oriented vertically upwards were installed on the original clamp bracket to firmly support the steel plate, ensuring its close contact with the underside of the rail track.

Per Hertzian contact theory, wheel-rail interaction within the elastic regime constitutes elliptical surface contact. The contact width ranges from 0.5 mm to 19 mm. A vertical load with

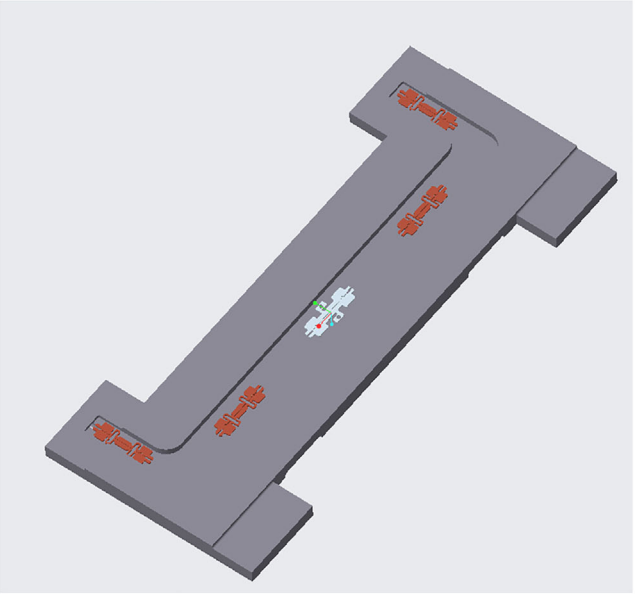

Figure 8. Composite sensor model. **Source(s):** Authors' own work

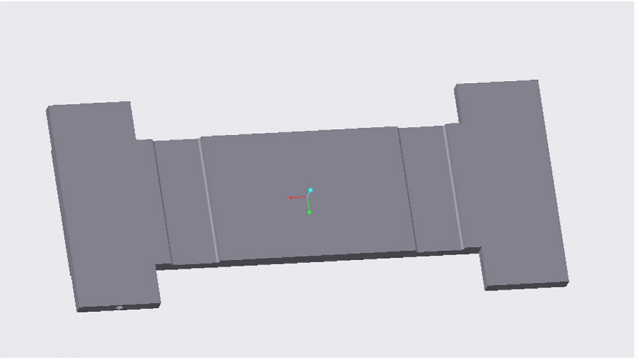

Figure 9. Back of composite sensor. **Source(s):** Authors' own work

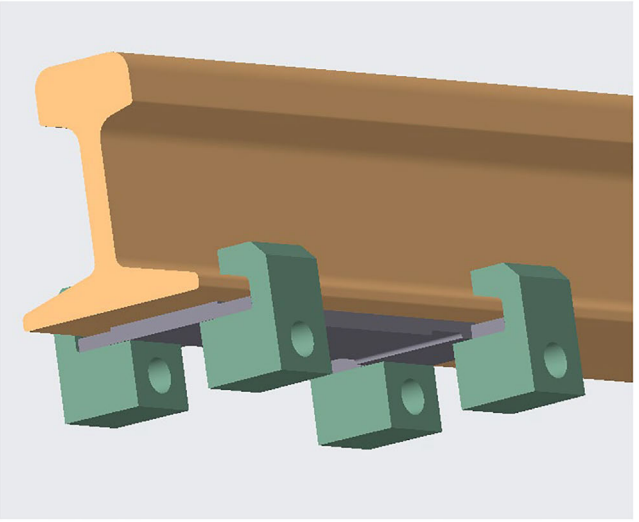

Figure 10. Composite sensor and track assembly model. **Source(s):** Authors' own work

6 mm minor axis length and corresponding major axis length was applied perpendicularly along the *z*-axis to simulate rail stress distribution during wheel passage. To characterize stress-strain transfer behavior and rail deformation, the load was imposed at the geometric center of the wheel-rail contact patch, followed by FEA of the rail model. The FEA was conducted to investigate the stress transfer characteristics between the sensor assembly and the rail. A model of a standard 60 kg/m steel rail was developed, as shown in the Figure 13. To evaluate the stress transfer efficiency at the axle counting position, the sensor module was simplified as a steel plate structure, as shown in the Figures 14 and 15. The FBG sensor is positioned beneath this steel plate, with the plate maintaining intimate contact with the rail base. The integrated sensor-rail assembly model is presented in Figure 16.

FEA of the simplified sensor model yielded the equivalent stress distribution shown in Figure 17. Directly beneath the applied loading, the base region of the rail exhibited a principal stress magnitude of 17.2 MPa, consistent with the stress generated by the load applied to the rail through the wheel. At the geometric centroid of the steel plate bottom surface

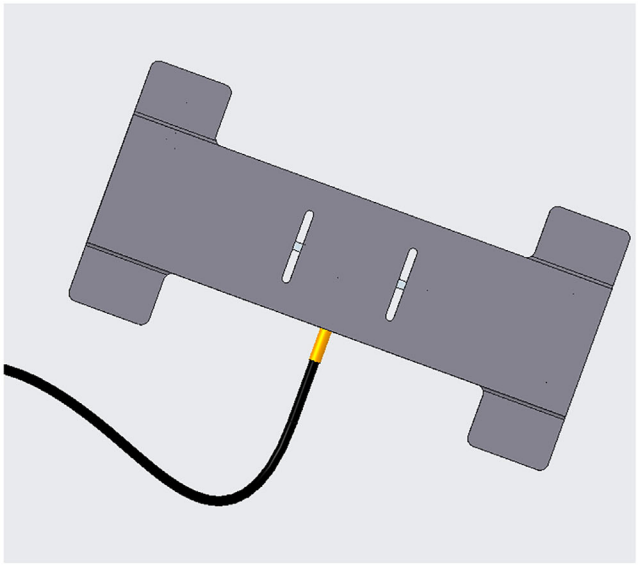

Figure 11. Upper surface of the slotted composite sensor. **Source(s):** Authors' own work

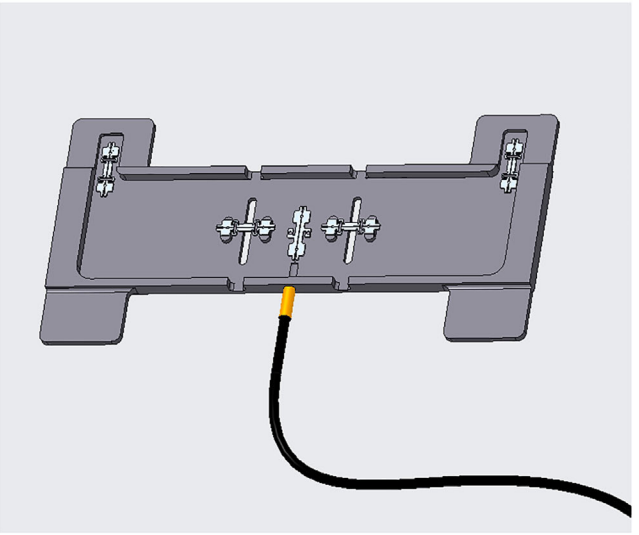

Figure 12. Bottom surface of the slotted composite sensor. **Source(s):** Authors' own work

(axle counting sensor location), the equivalent von Mises stress measured 2.6 MPa, that corresponds to a stress transfer efficiency of 15.1%. Within the elastic regime, stress and strain obey Hooke's law:

$$\sigma = \mathrm{E}\varepsilon \tag{2}$$

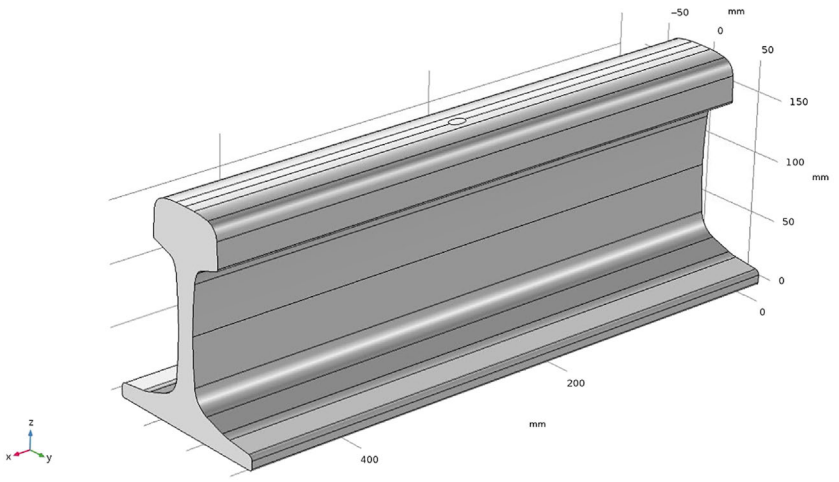

Figure 13. Rail model. **Source(s):** Authors' own work

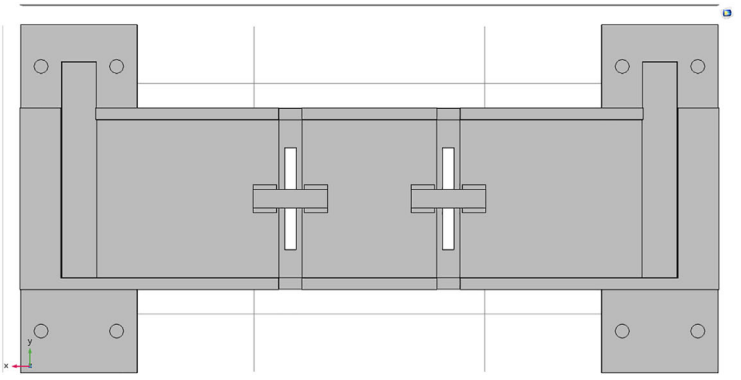

Figure 14. Bottom surface of the slotted composite sensor. **Source(s):** Authors' own work

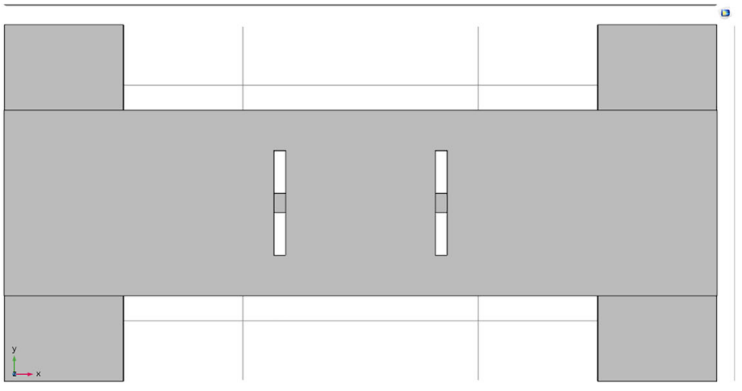

Figure 15. Upper surface of the slotted composite sensor. **Source(s):** Authors' own work

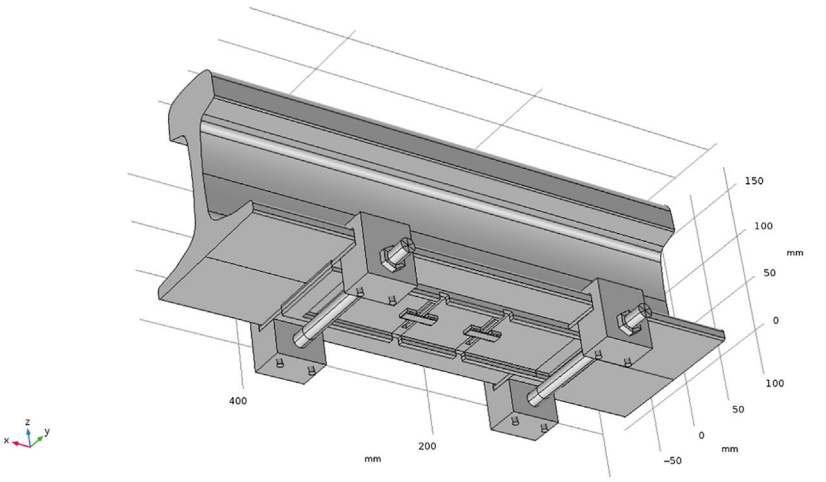

Figure 16. Slotted composite sensor and track assembly model. **Source(s):** Authors' own work

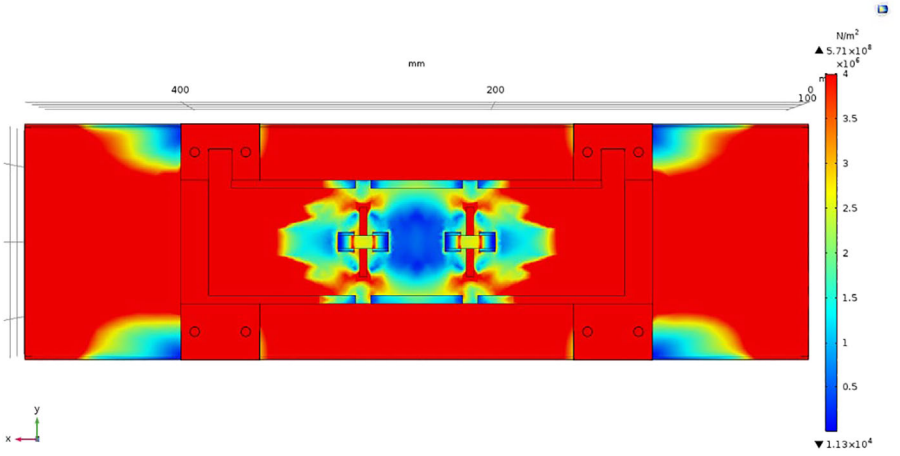

Figure 17. Von mises of the slotted composite sensor. **Source(s):** Authors' own work

where σ is stress, E is elastic modulus, and ε is strain. Then, the strain at the sensor position is approximately 13 $\mu\varepsilon$, and the sensor response is too small, which is not conducive to peak detection. Substituting the steel plate with a sensitive strain gauge can enhance stress transduction efficiency.

To achieve enhanced sensitization performance, two through-slots were machined from opposing sides at the axle counting sensor position (see Figures 18 and 19). This optimized configuration was subjected to FEA, with the resultant equivalent von Mises stress distribution detailed in Figure 20. For experimental validation, a steel plate replicating strain transduction behavior was mounted at the identical sensor location, recording 7.81 MPa stress and 39 $\mu\varepsilon$ strain. This corresponds to a stress transfer efficiency of 45.4%, representing a 200% improvement in strain sensitivity over the baseline model.

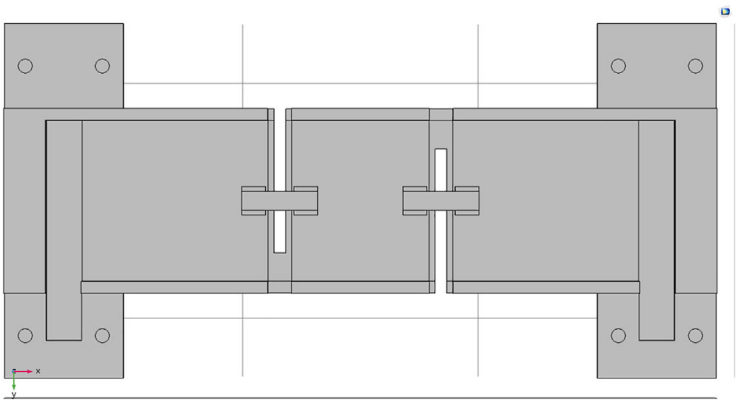

Figure 18. Bottom surface of the double-slotted composite sensor. **Source(s):** Authors' own work

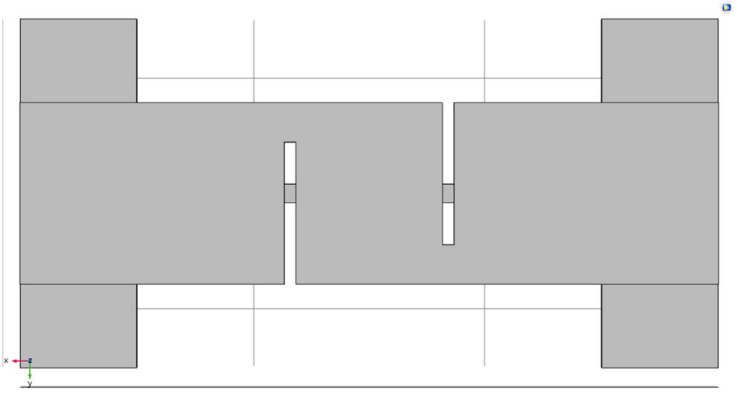

Figure 19. Upper surface of the double-slotted composite sensor. **Source(s):** Authors' own work

Based on the principle of strain concentration at geometric discontinuities, the axle counting sensor was relocated proximal to the slot opening edge to capitalize on enhanced deformation potential (see Figure 21). The reconfigured model was subjected to FEA, revealing an equivalent von Mises stress magnitude of 8.85 MPa at the sensor location (see Figure 22). This represents a 13.3% increase from the 7.81 MPa baseline value at the identical position, though the deviation falls within deviations. Consequently, design modification necessitates co-optimization with wiring constraints.

To evaluate potential adverse effects of biaxially oriented through-slots on deformation at the sensing location, a single-slot configuration was modeled (see Figure 23). FEA yielded an equivalent von Mises stress magnitude of 8.79 MPa at the axle counting sensor position (see Figure 24). This represents a statistically insignificant 12.5% deviation from the dual-slot configuration's 7.81 MPa, confirming that the dual-slot design induces no detrimental deformation effects.

To assess single-slot configuration effects, a sensor model incorporating slot-edge positioning was developed (see Figure 25). FEA revealed an equivalent von Mises stress magnitude of 9.15 MPa at the sensing location (see Figure 26). This represents a 3.39%

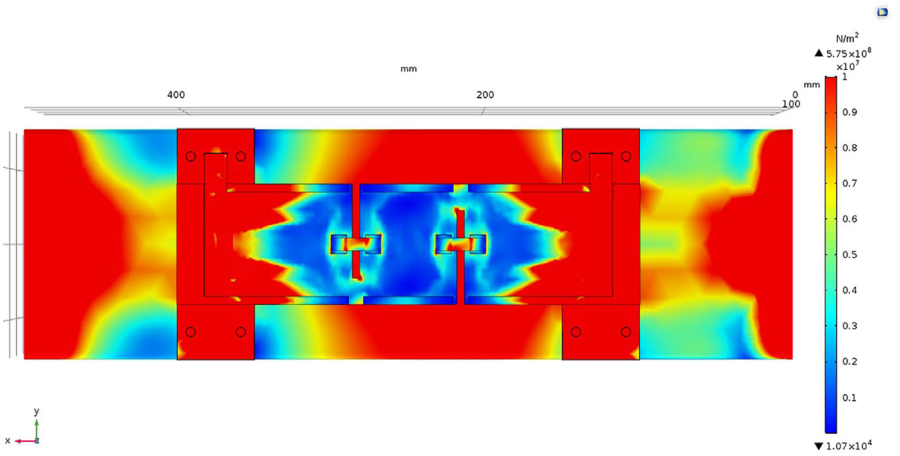

Figure 20. Von mises of the double-slotted composite sensor. **Source(s):** Authors' own work

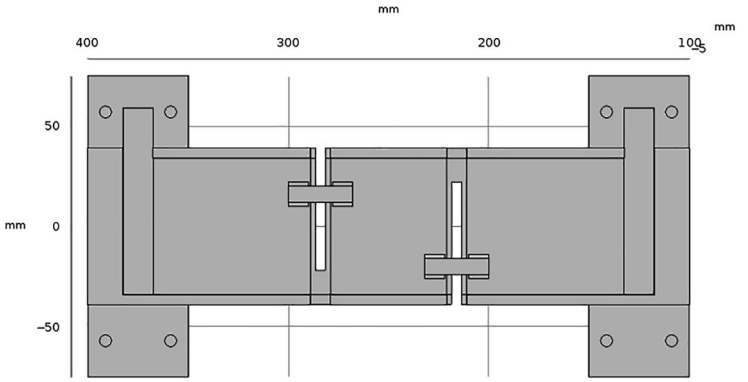

Figure 21. Bottom surface of the double-slotted composite sensor with a counting axis sensor located at the edge. **Source(s):** Authors' own work

increase relative to the dual-slot configuration's 8.85 MPa, confirming that biaxial slotting induces no detrimental deformation effects.

In prior simulations, wheel loading was centered over the composite sensor assembly. To assess off-center loading effects, a model with the axle positioned directly above the right axle counting sensor was developed (see Figure 27). The equivalent von Mises stress at this sensor location measured 7.06 MPa (see Figure 28), representing a 9.60% deviation from the dual-slot configuration's 7.81 MPa under centered loading. This confirms negligible deformation sensitivity to axle positioning variations.

Through comparative analysis of slot configurations, sensor positioning, and axle-sensor alignment effects on stress transfer characteristics, the following conclusions are substantiated:

(4) Opening the slots can effectively enhance stress transmission (increasing it by up to three times);

(5) Dual-slot configurations induce statistically insignificant stress variance;

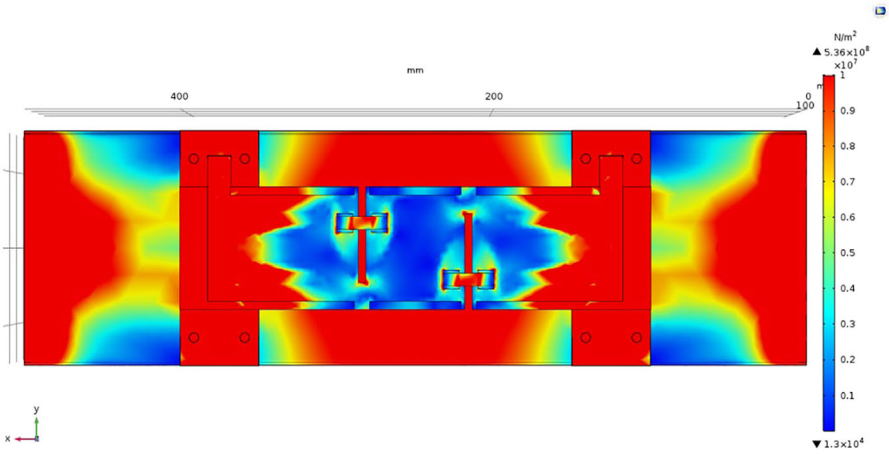

Figure 22. Von mises of a double-slotted composite sensor with a counting axis sensor located at the edge. **Source(s):** Authors' own work

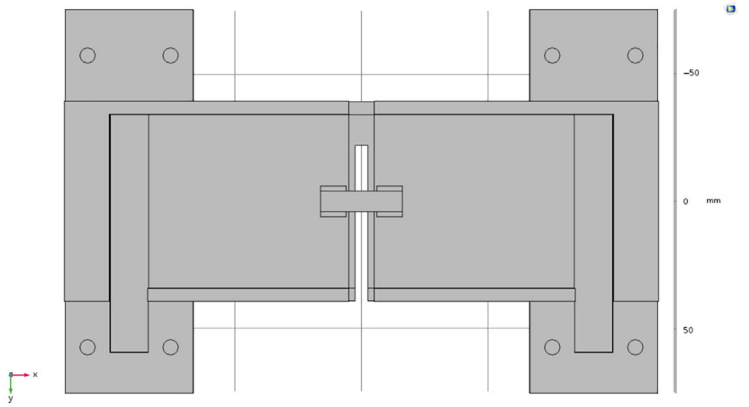

Figure 23. Bottom surface of the single-slotted composite sensor. **Source(s):** Authors' own work

(6) The placement of sensors relative to the edge of the slot causes stress modulation of ≤13.3%. The optimal sensor placement needs to be optimized in conjunction with wiring constraints and strain uniformity targets;

(7) The deviation between the axis and sensor position causes stress fluctuations of 9.6%, which can be considered insignificant.

5. Conclusions

Recent years have witnessed significant advancements in FBG applications for railway axle counting systems. However, extant research predominantly focused on theoretical modeling, stress analysis, and algorithmic optimization, with limited attention to sensor structural design

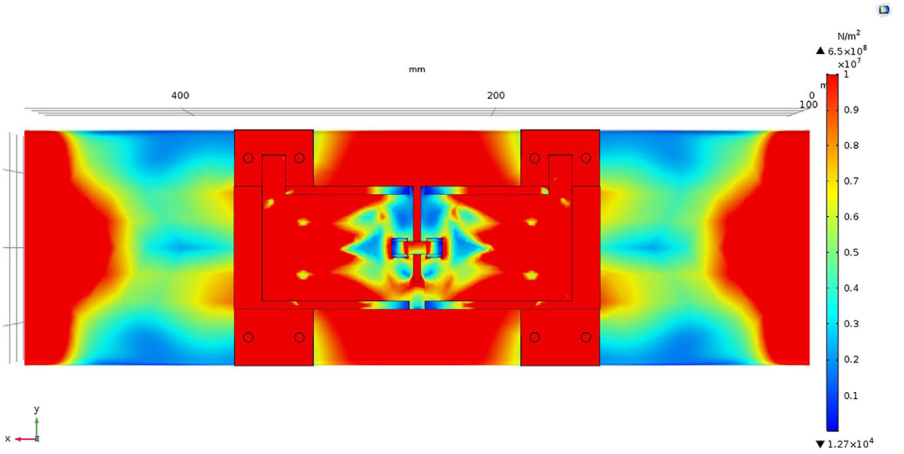

Figure 24. Von mises of the single-slotted composite sensor. **Source(s):** Authors' own work

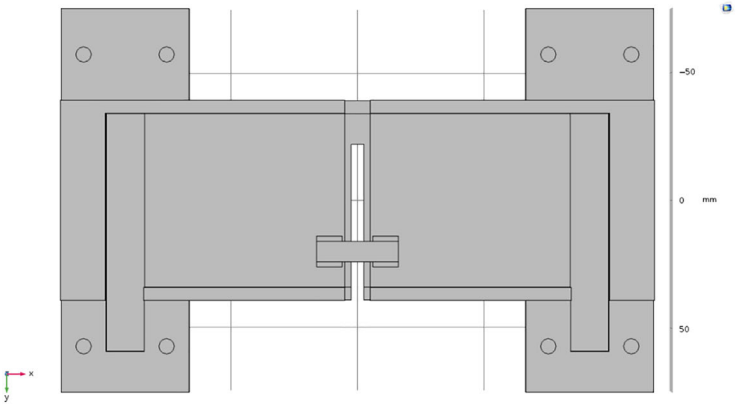

Figure 25. Bottom surface of the single-slotted composite sensor with a counting axis sensor located at the edge. **Source(s):** Authors' own work

addressing practical field requirements. To fulfill FBG axle sensor design requirements, a finite element model incorporating material properties, geometric configurations, and boundary conditions simulated train-rail interaction. Static load analysis yielded rail von Mises stress distributions, graphically depicting spatial stress magnitude and gradient patterns, providing crucial insights into the stress state of the rail. Analysis of the stress distribution map revealed that the regions with higher stress levels include the rail head, rail web, and rail base. Among these, the rail head and rail web are unsuitable for installing sensors that meet the requirements for long-term monitoring without damaging the rail itself. Peak stress locations were identified within each rail section through comparative analysis of equivalent von Mises stress and directional stress tensor components (x, y, z). This assessment established the base region as the optimal sensing location for transducer installation. Further analysis of the stress distribution at the rail base confirmed that the *y*-direction of the rail is the region with the highest stress component. This informed the design solution of installing the fiber optic grating sensor at the rail base, with the axle counting sensor's axis parallel to the rail direction.

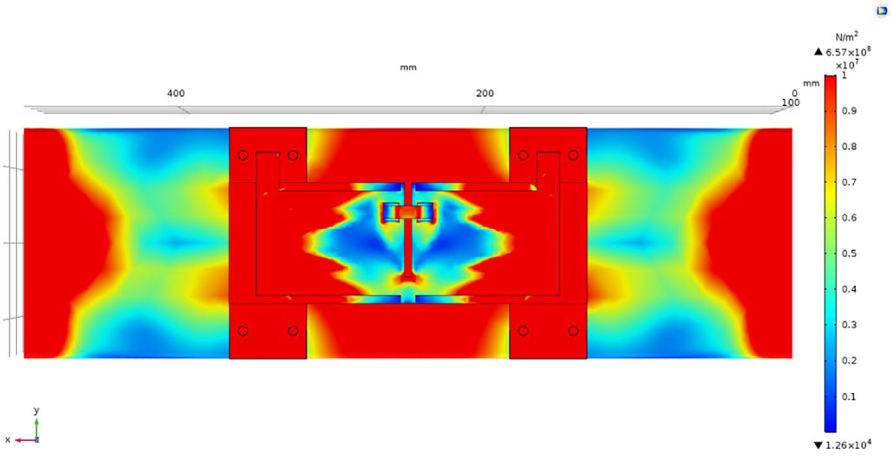

Figure 26. Von mises of the single-slotted composite sensor with a counting axis sensor located at the edge. **Source(s):** Authors' own work

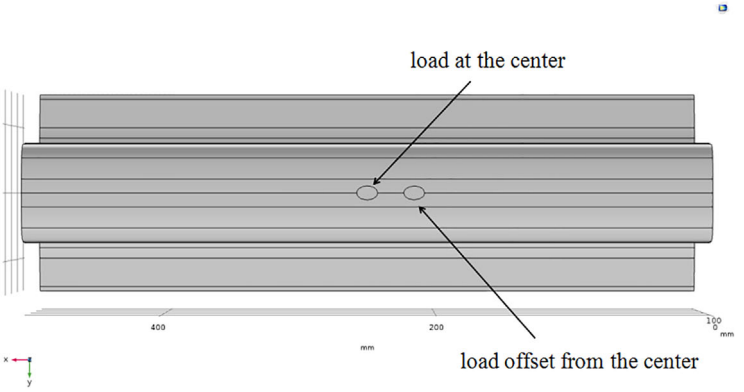

Figure 27. Load after rightward shift versus original load. **Source(s):** Authors' own work

A clip-on composite sensor has been designed for easy installation and maintenance, effectively protecting the fiber optic grating to ensure stable and reliable measurement performance in harsh environments. To further enhance measurement accuracy, the composite sensor is equipped with a temperature-compensated grating that monitors environmental temperature changes in real time, effectively eliminating the interference of temperature factors on the stress measurement results of the fiber optic grating, thereby significantly improving the accuracy of stress measurements. Additionally, to ensure the long-term stable operation of the sensor, an anti-detachment monitoring FBG is installed to monitor the installation status of the composite sensor in real time. Once any installation loosening is detected, an early warning signal is immediately issued, enabling staff to promptly take maintenance measures. The composite sensor was structurally optimized by cutting slots in the steel plate at the position of the axle sensor to enhance sensitivity. Stress transfer was increased to 3 times, reaching 7.81 MPa, with strain of 39 $\mu\varepsilon$. Given that rolling contact stresses induced by dynamic wheel loads during train operation typically exceed static loading by a factor of

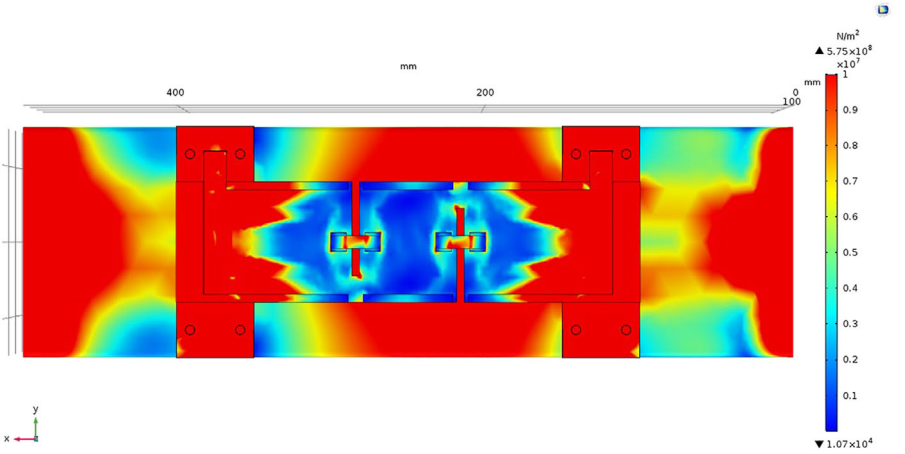

Figure 28. Von mises of the double-slotted composite sensor located directly above the right axle sensor.
Source(s): Authors' own work

1.2–1.5, and the implementation of sensitivity-enhanced strain transducers–as opposed to conventional steel plates–effectively amplifies strain transfer to FBG, operational axle counting sensors exhibited measurable strains exceeding 39 $\mu\varepsilon$. To validate the design rationality and performance reliability of the dual-slot composite sensor, FEA was conducted to quantify the stress magnitude at the axle sensor position of the dual-slot composite sensor. Additionally, FEA was performed on sensors with different structural configurations, including adjustments to the axle sensor position, number of slots, and axle position. The results confirmed that the designed composite sensor exhibited superior stress transfer characteristics satisfying FBG axle measurement system requirements.

Future work will implement transient dynamics simulations of train-rail interactions to characterize dynamic strain transients and spatial strain distributions under variable train mass/velocity profiles. Sensor topology will be optimized to enhance strain resolution and enable multi-parameter monitoring. Based on the sensor's dynamic response and measurement accuracy, an appropriate fiber optic grating wavelength demodulation rate will be selected, and an axle counting algorithm will be designed and tested on-site.

References

Cai, Y. W., Chen, B., & Chang, C. Y. (2024). Research on the strain gauge mounting scheme of track wheel force measurement system based on high-speed wheel/rail relationship test rig. *Railway Sciences*, *3*(4), 503–513. doi: 10.1108/rs-05-2024-0015.

Canning, J. (2008). Fibre gratings and devices for sensors and lasers. *Laser and Photonics Review*, *2*(4), 275–289. doi: 10.1002/lpor.200810010.

Ding, B. Y., Zhao, Q., Cheng, D. Y., & Du, D. W. (2024). Technology and application progress of fiber bragg grating pressure sensing. *Study on Optical Communications*, 3, 75–86.

Hajar, R., & Mounia, A. (2025). Investigating wheel–rail contact behavior on ballasted and non-ballasted tracks using finite element simulation. *Iranian Journal of Science and Technology, Transactions of Civil Engineering*, 1–20, (prepublish).

He, J., Wang, W. Q., Zhang, Q., Wang, W. K., & Yang, N. P. (2024). Analysis of rail corrugation deterioration behavior on a heavy-haul railway. *Proceedings - Institution of Mechanical Engineers*, *238*(9), 1133–1140. doi: 10.1177/09544097241262360.

Kacik, D., Martincek, I., Maciak, J., & Goraus, M. (2022). Fabry-pérot interferometer monitoring system for counting train axle. *IEEE Transactions on Instrumentation and Measurement*, *71*, 1–9. doi: 10.1109/tim.2022.3188032.

Lee, K. Y., Lee, K. K., & Ho, S. L. (2004). Exploration of using FBG sensor for axle counter in railway engineering. *WSEAS Transactions on Systems*, *3*(6), 2440–2447.

Li, W. L., Pan, J. J., & Fan, D. (2009). Data acquisition and processing for fiber grating train axle counting system. *Journal of Wuhan University of Technology*, *31*(2), 13–15.

Liu, Y. L. (2019). *Rsearch on magnetic field analysis and parameter optimization of unilateral axle counting sensor*. Harbin: Harbin Institute of Technology.

Liu, Y., Jian, S. S., Pei, L., & Yan, F. P. (2005). Research on the novel maglev train locating method based on fiber grating pressure sensor. *Journal of the China Railway Society*, *27*(5), 72–76.

Ni, X. (2022). *Research and Implementation of high stability fiber bragg grating track axle counter system*. Wuhan: Wuhan University of Technology.

Pan, J. J., Hou, W., Bao, C. W., Wang, L. Y., Lv, H. Y., & Zhou, W. (2022). Research on axle counting sensor based on fiber Bragg grating. In *Eighth Symposium on Novel Photoelectronic Detection Technology and Applications*, America. SPIE.

Velic, D., Krobath, M., Stocker, E., Ossberger, U., Gsodam, J., & Daves, W. (2023). A finite element modelling approach for the numerical analysis of switch rail contact loading and cyclic profile degradation. *Proceedings of the Institution of Mechanical Engineers, Part F: Journal of Rail and Rapid Transit*, *237*(2), 157–165. doi: 10.1177/09544097221095694.

Wang, J. N., Zhou, X. F., Liu, K., Wang, K. Y., & Jing, L. (2025). Wheel-rail dynamic interaction induced by tread spalling integrating with pre-fatigue damage of materials. *Computers & Structures*, *308*, 107640. doi: 10.1016/j.compstruc.2024.107640.

Wei, C. L., Lai, C. C., Liu, S. Y., Chung, W. H., Ho, T. K., Tam, H. Y., . . . Lee, K. Y. (2010). A Fiber bragg grating sensor system for train axle counting. *IEEE Sensors Journal*, *10*(12), 1905–1912. doi: 10.1109/jsen.2010.2049199.

Wu, C. X., Zhang, L., Yang, F., Wang, S., Zhang, T. F., & Wang, D. (2024). Research on axle counter system based on fiber bragg grating sensing technology. *Railway signaling & communication engineering*, *21*(8), 9–14, 91.

Yan, L. S., Zhang, Z. T., Wang, P., Pan, W., Guo, L. K., Luo, B., . . . Zhao, G. G. (2011). Fiber sensors for strain measurements and axle counting in high-speed railway applications. *IEEE Sensors Journal*, *11*(7), 1587–1594. doi: 10.1109/jsen.2010.2086058.

Yu, Q., He, D. W., Wang, Y. S., & Wang, P. F. (2014). Axle counter for high-speed railway based on fibre Bragg grating sensor and algorithm optimization for peak searching. In *7th International Symposium on Advanced Optical Manufacturing and Testing Technologies (AOMATT 2014)*, Harbin, China (pp. 92850D). SPIE Digital Library.

Zhang, S. L., & Yan, Y. (2019). Monitoring system of track circuit system based on optical fiber sensor. *Journal of Shijiazhuang Tiedao University (Natural Science Edition)*, *32*(3), 107–112.

Zhang, L., Pan, J. J., Wang, Z. X., Zhou, R., Lin, J. F., & Wu, C. X. (2020). An intensity demodulated FBG axle counter system. In *2020 International Conference on Computer, Network, Communication and Information Systems (CNCI 2020)*, Canada. Clausius Scientific Press.

Corresponding author
Longsheng Wang can be contacted at: lshwang@aliyun.com

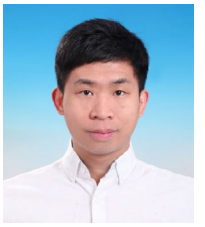

Longsheng Wang received his Ph.D degree from Beijing Jiaotong University in 2016. He is currently working at Signal & Communication Research Institute, China Academy of Railway Sciences Corporation Limited. His current research interests include Railway Signal Control, Cloud-Based Signalling System, automatic train operation and model predictive control.